AIAA JOURNAL
Vol. 33, No. 2, February 1995

Study of Subsonic Base Cavity Flowfield Structure Using Particle Image Velocimetry

Michael J. Molezzi* and J. Craig Dutton†
University of Illinois at Urbana–Champaign, Urbana, Illinois 61801

A new particle image velocimetry system has been used to study the near-wake structure of a two-dimensional base in subsonic flow to determine the fluid dynamic mechanisms of observed base drag reduction in the presence of a base cavity. Experiments were done over a range of freestream Mach numbers up to 0.8, including local flowfield velocities over 300 m/s. Effects of the base cavity on the von Kármán vortex street wake were found to be related to the expansion and diffusion of vortices near the cavity, although the effects are of small magnitude and no significant change in the vortex formation location or path was observed. The base cavity effects are also less significant at higher freestream velocities due to the formation of vortices further downstream from the base. The base cavity drag reduction was found to be mainly due to the displacement of the base surface to a location upstream of the low-pressure wake vortices, with only a slight modification in the vortex street itself.

Introduction

THE separated flow past a two-dimensional body at subsonic speed and large Reynolds number forms a wake structure made up of alternately shed vortices known as the von Kármán vortex street. This commonly occurring structure has been the subject of numerous studies beginning with von Kármán's first theoretical analysis of vortex streets.[1] A significant feature of this flowfield is the interaction of the low-pressure vortices in the near wake with the downstream surface or base of the body, inducing a net streamwise pressure force on the body known as base drag. The base drag is typically a significant component of total drag, even for slender bodies with a finite thickness base. For this reason, drag reduction methods based on the modification of the vortex street have received much attention.

One effective drag reduction method is the use of a base cavity, which is the subject of this study. It has been shown experimentally that the presence of a solid-walled cavity in the base of a slender two-dimensional body (see Fig. 1) increases the base pressure, resulting in base drag reduction of up to 30%.[2–5] Other effects of a base cavity that have been experimentally observed include an increase in vortex shedding frequency or Strouhal number as compared with a blunt base[4,5] and limited drag improvement for a cavity depth beyond approximately half the base height.

The mechanism of drag reduction due to base cavities is as yet unclear, although several theories have been proposed, all of which imply some modification of vortex formation location and reduction in vortex strength. The earliest published base cavity experiments were done by Nash et al.[2] They proposed that, although a vortex or eddy may not be completely trapped by the cavity, the cavity does have a stabilizing effect on standing eddies near the base, implying that the vortices form at least partially within the cavity where they are affected by the cavity walls. Pollock[3] performed experiments based on theoretical work by Ringleb[6] who suggested that a stable vortex may be trapped in a cavity, causing the wake to revert to a steady flow. Pollock used a special asymmetric cusp-shaped cavity that showed no advantage in drag reduction over a rectangular cavity, in effect disproving Ringleb's theory. In a study of resonance effects on vortex shedding, Wood[7] showed that resonance of the base at the vortex shedding frequency causes vortex formation within the cavity, whereas formation normally occurs outside the cavity. He concluded that the drag reduction observed for base cavities must be due to some resonance or vibration in the flowfield, moving the vortices into the cavity where the solid walls restrict vortex growth and inhibit the strength of successive vortices.

A study of axisymmetric base cavities by Compton[8] suggested that recirculation within the cavity forms a coflowing stream at the cavity edge that interacts with the separated freestream, reducing the vorticity of the separated shear layer. In a subsequent study of axisymmetric base cavities, Morel[9] suggested that the coflowing stream could be an important effect in two-dimensional geometries as well. More recently, Kruiswyk and Dutton[4] used a combination of pressure measurements and flow visualization techniques to conclude that, although vortex motion does not extend into the cavity, oscillating airflow at the cavity boundary increases fluid mixing in the near wake, thereby reducing vortex strength. Their results concerning the change in base pressure and vortex shedding frequency due to a base cavity are shown in Table 1. The base cavity was rectangular with a streamwise depth equal to half the base height. A base cavity with a depth of one full base height was also used, but the results were similar to those of the half base height cavity. The results in Table 1 show an increase of 10–14% in the base pressure coefficient, which is nondimensionalized by reference conditions in the flow just before separation near the downstream edge of the base. The relative increase in the Strouhal number (vortex shedding frequency) is smaller, although still significant. Another evident feature is that both effects are largest at the lowest freestream Mach number. The experimental conditions used in the present study match those used by Kruiswyk and Dutton[4] to facilitate comparison of data.

Two notable computational simulations of two-dimensional base cavity flows have also been done. Rudy[10] obtained finite difference Navier-Stokes solutions using base configurations and freestream Mach numbers of 0.4 and 0.6 that matched those of Kruiswyk and Dutton.[4] However, Rudy's simulations were laminar, using freestream Reynolds numbers (based on base height) of 700 and 962 that are significantly lower than experimental values. Clements and Maull[5] used an inviscid discrete vortex method for simulations of their experimental results. Rudy's results more accurately predicted the experimentally measured base pressure increase due to a cavity, but both simulations showed vortex formation within the cavity and a decrease in shedding frequency due to the cavity, which disagrees with experimental results. Rudy concluded that the observed increase in base pressure with a cavity was mainly due to the physical displacement of the base surface away from the low-pressure vortices.

Presented as Paper 93-3040 at the AIAA 24th Fluid Dynamics Conference, Orlando, FL, July 4–9, 1993; received Oct. 1, 1993; revision received Aug. 12, 1994; accepted for publication Aug. 28, 1994.

*Research Assistant, Department of Mechanical and Industrial Engineering; currently Staff Engineer, General Electric Corporate Research and Development, One River Rd., K1-ES121, Schenectady, NY 12309. Member AIAA.

†Professor, Department of Mechanical and Industrial Engineering. Associate Fellow AIAA.

Table 1 Base pressure and shedding frequency effects due to base cavity (taken from Kruiswyk and Dutton[4])

Freestream Mach no., M_∞	Freestream Reynolds no., Re_∞	Base pressure coefficient C_p increase,%	Strouhal no. St Increase, %
0.4	1.36×10^5	14.1	6.53
0.6	1.82×10^5	9.8	3.65
0.8	2.09×10^5	10.3	2.57

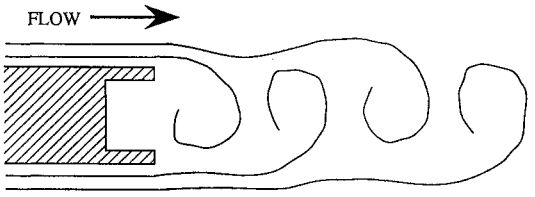

Fig. 1 Typical two-dimensional base cavity and subsonic vortex street wake.

The work presented here will take advantage of both the new results available from particle image velocimetry (PIV) and the extensive experimental and computational data available from Kruiswyk and Dutton[4] and Rudy,[10] respectively. The ability to directly compare results from several techniques for similar base geometries and flow conditions will allow a thorough analysis of the effects of a base cavity on the structure and properties of the flowfield, leading to a better understanding of the mechanisms of drag reduction.

Equipment

Test Section

Experiments for this study were performed in a previously fabricated transonic wind tunnel (Fig. 2) based on a design described by Little and Cubbage.[11] The tunnel has a 4 × 4 in. (101.6 × 101.6 mm) test section with solid sidewalls and slotted upper and lower inner walls to relieve the blockage effect of models in the subsonic to transonic speed range. Six-in.-diam round windows are mounted in both sidewalls to allow visualization of the downstream end and near wake of a base model. The tunnel is a blowdown type supplied with compressed dry air from a 140 m^3 tank farm at 120 psia. The base model (Fig. 2) consists of an interchangeable afterbody mounted on a wedge-shaped forebody. Trip wires are mounted on the top and bottom surfaces near the upstream edge to assure a uniformly turbulent boundary layer at separation. When mounted in the test section, the upstream edge is located approximately 17 in. (432 mm) downstream of the wind tunnel entrance with approximately 0.75 in. (19 mm) of the downstream end of the model visible through the side windows. The afterbodies used are a blunt base and a rectangular base cavity with a depth of half the base height. The wind tunnel and base models are the same as those used by Kruiswyk and Dutton.[4]

Modifications have been made to the original wind tunnel for the flow seeding and optical access necessary for this study. Slot-shaped upper and lower windows have been fabricated and installed in the outer tunnel walls for access with a vertically propagating planar laser sheet. The sheet passes through the lower window and through one of the streamwise slots of the inner wall to enter the test section. The arrangement of the wall slots requires the position of the sheet to be 10 mm off the tunnel centerline in the spanwise direction, but surface flow visualization on the base model[4] and laser Doppler velocimetry (LDV) data in the near wake[12] indicate no significant variation of the flow within 10 mm of the centerline. Delivery of silicone oil droplet seeding for PIV is done by two TSI six-jet atomizers feeding a single 3/4-in. o.d. tube that enters the stagnation chamber. Flow from the stagnation chamber passes through a pair of screens (44 × 44 mesh screen with 57% open area) and enters an enclosure at the nozzle entrance to reduce turbulence. The atomized silicone oil is then injected through a manifold tube with a series of holes directed downstream and oriented in a transverse (vertical) plane aligned with the illuminating laser sheet. The flow then passes

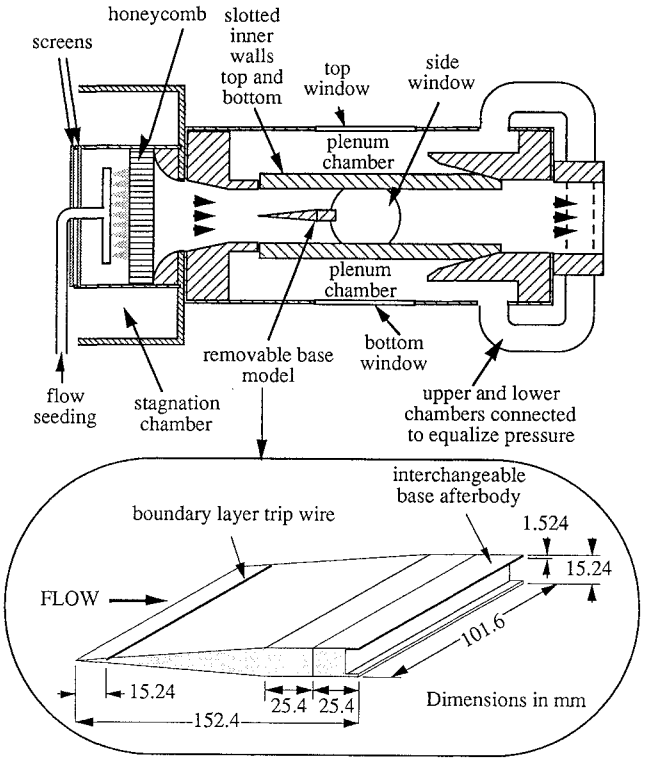

Fig. 2 Base flow test section and base model.

through a 2-in.-long section of honeycomb with a 3/16-in. cell diameter to further reduce turbulent fluctuations. The seed injection is done downstream of the screens due to experience with LDV indicating that silicone oil droplets tend to build up on screens, causing large drops to form and burst off, which bias velocity measurements. LDV data from the final tunnel configuration indicate tunnel-empty turbulence intensities of less than 1% at the freestream conditions used in this study.

PIV System

To meet the objectives set forth for this study, data were obtained with a nonintrusive velocity measurement technique called particle image velocimetry (PIV). PIV is performed by illuminating a seeded flowfield with a planar laser sheet that is pulsed at a known time interval, forming two or more sequential images of each seed particle within the light sheet (Fig. 3). The particle images are captured on film or another medium; then the local image separations and, therefore, velocities can be determined for the entire plane. Unlike pointwise techniques such as LDV, which provides statistical velocity data on a point-by-point basis, PIV can quantitatively identify instantaneous flow structures that may be random in nature but important to the overall behavior of the flow. PIV also reveals planar views of three-dimensional flow structures that are smeared by volume integration inherent in techniques such as schlieren photography. A detailed discussion of the design, development, and validation of the automated PIV system used in this study can be found in Refs. 12 and 13.

The current study used a beam thickness of 1.2 mm and width of 64 mm at the test section with a uniform interrogation region for each velocity measurement of 1 × 1 mm in the frame of reference of

Table 2 Experimental conditions

Freestream Mach no., M_∞	Reference Mach no., M_{ref}	Base configuration	Freestream Reynolds no., Re_∞	Notation
0.4	0.49	Blunt	1.36×10^5	M4b
0.4	0.49	Half-height cavity	1.36×10^5	M4c
0.6	0.74	Blunt	1.82×10^5	M6b
0.6	0.74	Half-height cavity	1.82×10^5	M6c
0.8	0.88	Blunt	2.09×10^5	M8b
0.8	0.88	Half-height cavity	2.09×10^5	M8c

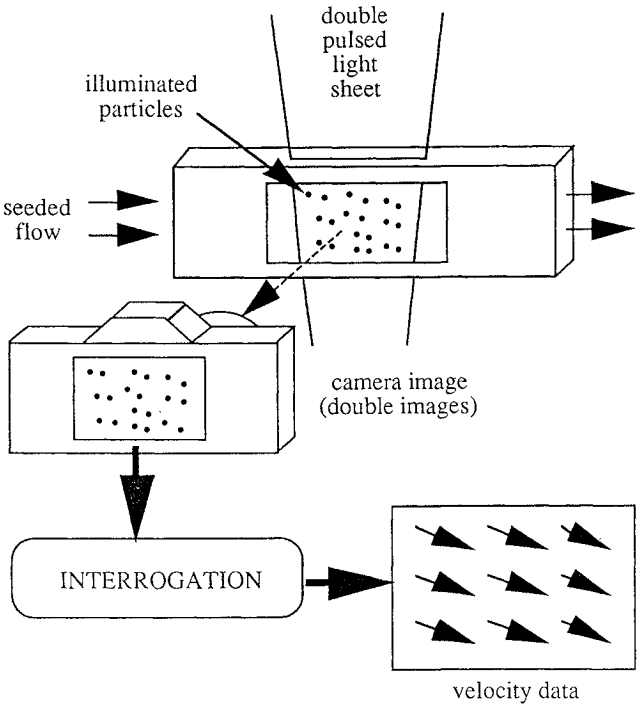

Fig. 3 Principle of PIV.

the test section. The probe volume is therefore 1 × 1 mm (spot size) by 1.2 mm (laser sheet thickness) or 1.2 mm.[3] Velocity vectors were determined on a grid with an increment of 0.5 mm in each direction (overlapping spots) to prevent biasing due to small-scale motions in the flowfield. The upstream edge of the vertically propagating beam passes just downstream of the aft edge of the base to avoid intense reflections from the base surfaces, thus preventing acquisition of PIV data within the base cavity.

Validation experiments have been performed with this PIV system using both simulations and high-speed flow experiments, indicating a maximum total error in raw PIV velocity measurements of less than 3%.[12] A large portion of this total is due to random error, which is reduced by processing operations performed on the raw data.[12,14]

Results and Discussion

Experimental Conditions

Experiments were initially performed with two base configurations at three freestream velocity conditions, resulting in six cases. Flow conditions for each case were determined by running the test section without the base model. The test section flow velocity was measured as a function of wind-tunnel stagnation pressure, allowing the appropriate stagnation pressure to be determined for each desired freestream velocity condition. This stagnation pressure was maintained for the corresponding experiments with the base model. A summary of the flow conditions and base configurations used in this study is shown in Table 2, including the freestream Reynolds number based on freestream velocity and base height, and shorthand notations for each case. As mentioned previously, these cases match those used by Kruiswyk and Dutton[4] and the Mach 0.4 and 0.6 freestream conditions used by Rudy[10] with similar base configurations.

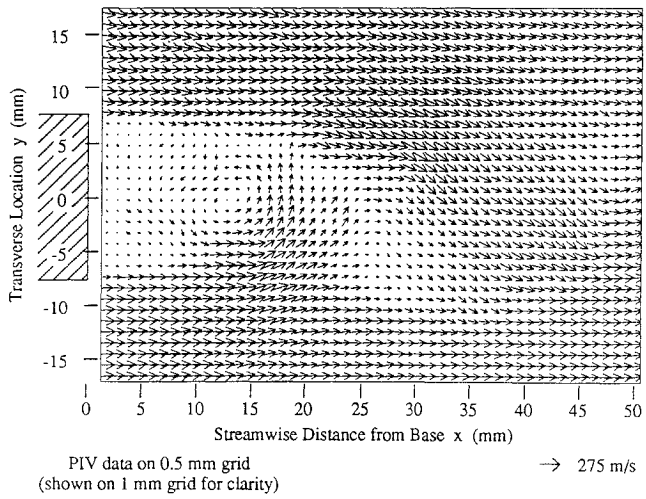

Fig. 4 M6b processed velocity vector plot.

As expected from inviscid flow theory, the measured velocity just outside the boundary layer at the downstream edge of the base (reference Mach number in Table 2) is greater than the associated freestream velocity due to local compression of streamlines near the body. The mean measured reference Mach numbers for each case were found to match the reference Mach numbers quoted by Kruiswyk and Dutton[4] for the associated freestream conditions. The velocity data from individual flowfield realizations showed some variation from the desired reference velocities (maximum 9%) due to the lack of tunnel control valve resolution at the small stagnation pressures required and due to changes in the stagnation temperature of the supply air from run to run. The velocity data from each flowfield realization were therefore scaled to account for these variations.

Individual Flowfield Realizations

Fifteen flowfield realizations were obtained for each of the Mach 0.4 and Mach 0.6 cases listed. Realizations were also obtained for each of the Mach 0.8 cases, but difficulties with seeding density in the vortex street prevents the use of those cases in the quantitative analysis presented here.[12] Each individual realization consists of an array of 6831 (99 × 69) instantaneous velocity vectors with 0.5-mm spacing in the streamwise and transverse directions. By defining the coordinate system as positive x in the streamwise direction and positive y in the transverse direction with the origin at the center of the downstream base edge, each realization covers the wake from $x = 1$ to 50 mm and from $y = -17$ to 17 mm. This region extends 2.2 base heights in the transverse direction and 3.3 base heights downstream of the aft edge of the base.

The velocity vector plot from a single Mach 0.6 blunt base (M6b) realization is shown in Fig. 4. As noted in the figure, only every other vector in each direction is plotted for the sake of clarity. Processing of the velocity data includes automated elimination of invalid velocity vectors (2–8% of total) that are caused by photographic imperfections, lack of particle images, and other effects. Interpolation is used to replace invalid data, and then a low-pass spatial filter smooths the data to eliminate any high-frequency random error.[12,14]

Figure 4 reveals some of basic features of the flowfield, including the presence of distinct alternating vortices. The first counter

Table 3 Base flow shear layer length and separation

Experimental case	Average shear layer streamwise length, mm	Cavity % change	Shear layer endpoint transverse separation, mm	Cavity % change
M4b	6.9	—	13.0	—
M4c	6.8	−1.4	12.5	−3.8
M6b	8.0	—	13.5	—
M6c	7.4	−7.5	12.8	−5.2

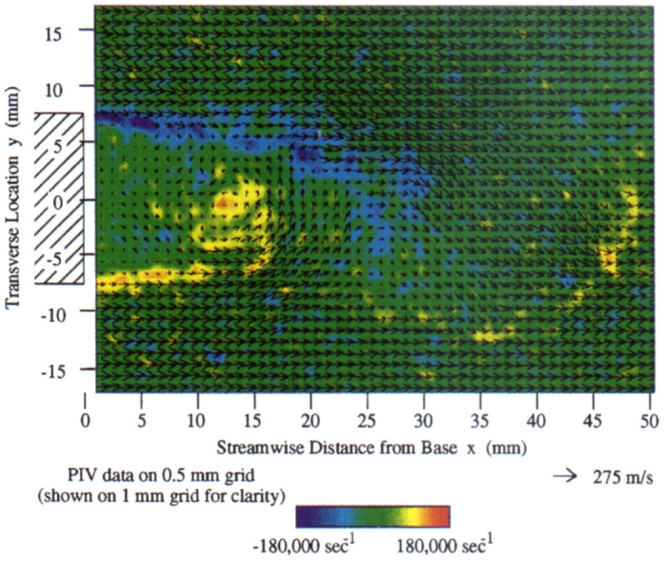

Fig. 5 M6b color vorticity plot with velocity vector overlay.

clockwise vortex near the base is clearly seen, whereas the structure of the next two vortices is less distinct due to increasing convective velocity in the downstream direction. The separated region near the base is also evident, with low velocity magnitudes immediately downstream of the base edge and significant upstream fluid motion at the first fully formed vortex. There is also evidence of turbulence throughout the flowfield, with irregularities in the vortex motion, especially near the base edge.

To analyze vortex location and strength, the out-of-plane vorticity

$$\omega_z = \left(\frac{\partial v}{\partial x} - \frac{\partial u}{\partial y} \right) \tag{1}$$

was computed for each flowfield realization. This was done by central differencing of the original velocity data. A color plot of vorticity with overlaid velocity vectors corresponding to Fig. 4 is shown in Fig. 5. These data present a new capability for quantitatively analyzing separated compressible flow structure that has to this point been impossible. One of the notable features in Fig. 5, which holds for all experimental conditions, is the significant fragmentation of the vortices as they shed from the separated shear layers at the aft edge of the base. This is indicative of the high level of boundary-layer turbulence before separation, confirmed by boundary-layer turbulence intensity measurements of up to 5% using LDV,[12] and its effect on the turbulent structure of the wake. Fast response pressure measurements made in the wake by Kruiswyk and Dutton[4] also showed a wide distribution of frequencies around the vortex shedding frequency, indicating the superposition of the vortex street on a random turbulent flowfield. Turbulence energy is therefore transferred in the wake from the large-scale vortices to smaller scales, causing the gradual breakdown of distinct vortices as they travel downstream.

Vorticity Statistics

As mentioned earlier, previous theories regarding the mechanism of base cavity drag reduction all hinge on some modification of vortex strength and/or position. For this reason, it is desirable to use the vorticity data now available to examine vortex path and strength, both with and without base cavities. Because of the turbulent nature of the flowfield and the resulting vortex fragmentation discussed previously, it is rather difficult to select a particular location for each vortex in an instantaneous realization. Therefore, a statistical method was adopted to estimate vortex path and strength. Because of the alternate shedding of the wake vortices, successive vortices have peak vorticity values ω_z of alternating sign, causing the mean vorticity to go to zero where the opposing vortex paths overlap. Since only the vorticity magnitude is necessary for the determination of vortex strength and path, it was decided to derive the root mean square (rms) vorticity for each experimental case, which is defined at each flowfield location (x, y) by

$$\omega_{\text{rms}}(x, y) = \left[\frac{\sum_{i=1}^{N} [\omega_z(x, y)]_i^2}{N} \right]^{\frac{1}{2}} \tag{2}$$

where the index i represents each individual realization for the experimental case of interest and N is the total number of realizations, or 15.

The results for the M4b, M4c, M6b, and M6c cases (see Table 2) are shown in Fig. 6. These plots show the region within approximately one base height of the aft edge to concentrate on the notable features. Although some data scatter is present due to the turbulence level and limited ensemble size, these plots do reveal useful information about cavity effects. One of the first noticeable features is the presence of the free shear layers at each separation point and their extension into the wake. At a point less than one-half base height downstream, they rapidly lose strength, indicating the mean location at which free vortices break off into the wake, or the vortex formation location. Lines have been included on the plots to identify the mean shear layer location, shape, and length. Each line was determined by a curvefit to the peak vorticity values in the shear layer, with the line terminating at the point where the vorticity drops below 67% of the maximum scale, or 67,000 s^{-1} for the M4b and M4c cases, and 100,000 s^{-1} for the M6b and M6c cases. This allows a relative comparison of the shear layer lengths between all four cases.

Table 3 shows the average shear layer length and the transverse separation distance of the shear layer endpoints for each case shown in Fig. 6. Although the average shear layer length is 0.6 mm shorter for the M6c case than the M6b case, the difference of 0.1 mm is not significant for the Mach 0.4 cases. The asymmetry in the shear layers propagating from the upper and lower base corners for a given case also prevents drawing any firm conclusion of a change in vortex formation location due to the cavity, although wake static pressure data were used by Kruiswyk and Dutton[4] to conclude that vortex formation occurs further downstream due to the cavity for a Mach 0.4 freestream velocity.

Figure 6 does, however, reveal that the angle of convergence of the shear layers toward the transverse centerline appears steeper for the base cavity cases than for the blunt base. There may also be a slight increase in shear layer curvature, although it is difficult to determine conclusively. Increased shear layer curvature would indicate a larger pressure gradient across the shear layer, which would, in turn, imply that the cavity causes lower mean static pressure in the region just inside the shear layer and just past the separation point. However, this must be only a local effect confined near the shear layer, since the cavity has been shown in previous research to increase the mean pressure over the base surface, which is upstream of the shear layers inside the cavity.

Convergence of the shear layers causes the transverse separation distance between the two shear layers to be reduced at their endpoints (see Table 3), explaining the increase in shedding frequency

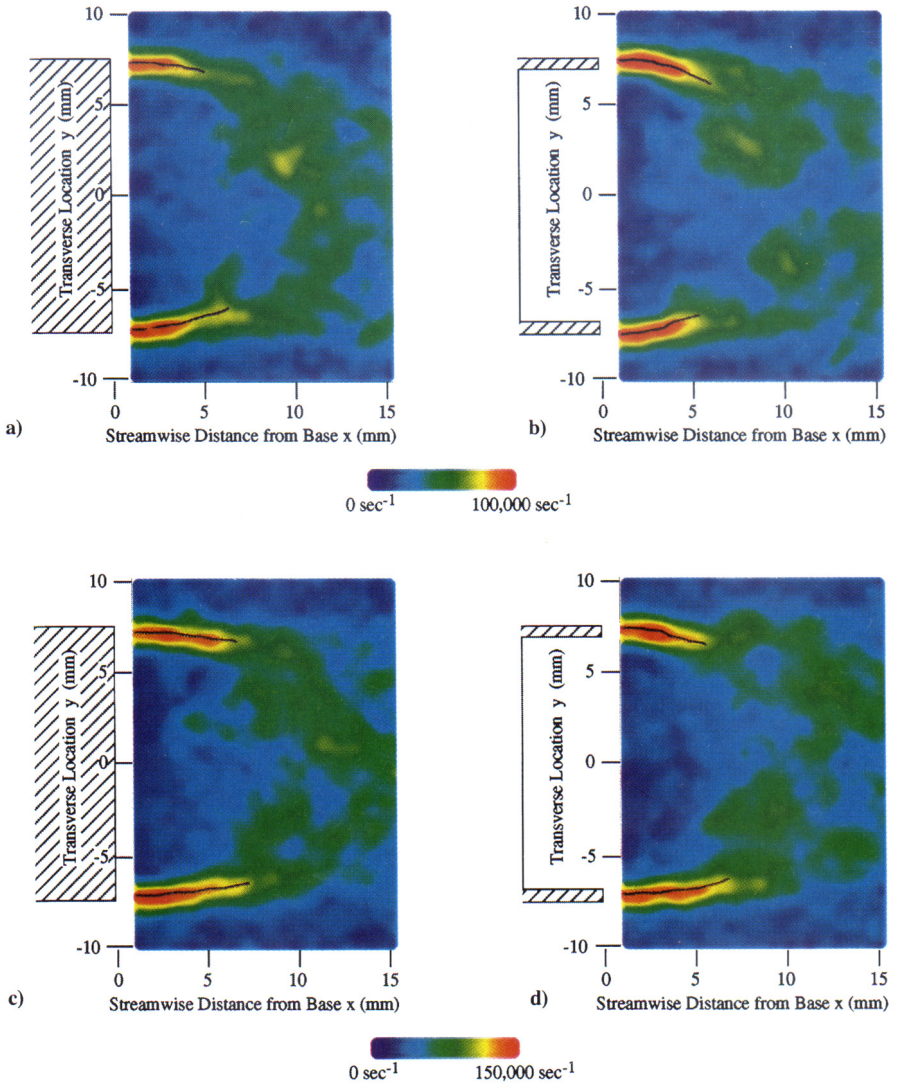

Fig. 6 Enlarged color rms vorticity plots indicating shear layers: a) M4b b) M4c, c) M6b, and d) M6c.

observed by Kruiswyk and Dutton[4] for the base cavity (see Table 1). As stated by Fage and Johansen,[15] the shedding frequency in a vortex street is inversely proportional to the separation distance of the shear layers in the wake. When the shear layer separation is reduced in the base cavity wake due to convergence, it follows that the shedding frequency increases.

In examining the vortex path just downstream of the shear layers, reduced vortex strength due to the base cavity can be seen in Fig. 6 for both freestream Mach numbers. In an effort to quantify this result, the spatially averaged rms vorticity was calculated for each case in Fig. 6 over a region extending between the two shear layer endpoints (in the transverse direction) and extending from the longest shear layer endpoint to 7.5 mm downstream of that endpoint (in the streamwise direction). This region was chosen to uniformly cover the initial vortex path for each case. The results are shown in Table 4. Although the data scatter in Fig. 6 makes small differences difficult to determine visually, the data in Table 4 show that the average rms vorticity level is indeed reduced by the cavity for both freestream Mach numbers, implying a small decrease in vortex strength.

Finally, any effect of the base cavity on mean vortex path is not clear from Fig. 6, although it is evident that turbulence causes the vortex path to be somewhat random, since the rms vorticity magnitude peaks are widely scattered in the wake for all cases.

The effects of increasing Mach number on the shear layers include a small increase in shear layer separation (see Table 3) that seems to be caused by a reduction in both the initial convergence angle and curvature of the shear layers, and can be attributed to increased streamwise momentum in the fluid stream outside the wake. The shear layers are also extended by approximately 1 mm for the Mach 0.6 freestream cases vs Mach 0.4, causing the vortex formation to occur further downstream of the base edge. However, any change in vortex path downstream of the shear layers due to the increase in freestream velocity is not evident from these data. Displacement of the vortex formation location further downstream of the base would serve to explain the reduced effectiveness of the cavity at higher Mach numbers as shown by Kruiswyk and Dutton[4] (see Table 1). As the vortices form further away from the base at higher Mach numbers, their effect on the pressure at the base surface is reduced, causing any modification of the vortex street due to the cavity to have less relative effect on the base pressure.

Table 4 Base flow near-wake vortex strength

Experimental case	Spatially averaged rms vorticity, s^{-1}	Cavity % change
M4b	42,590	——
M4c	40,890	−4.0
M6b	66,120	——
M6c	62,490	−5.5

Instantaneous Wake Structure

Further information on base cavity wake effects can be obtained by comparing the instantaneous wake structure for the blunt base and base cavity at a similar point in the vortex shedding cycle. For

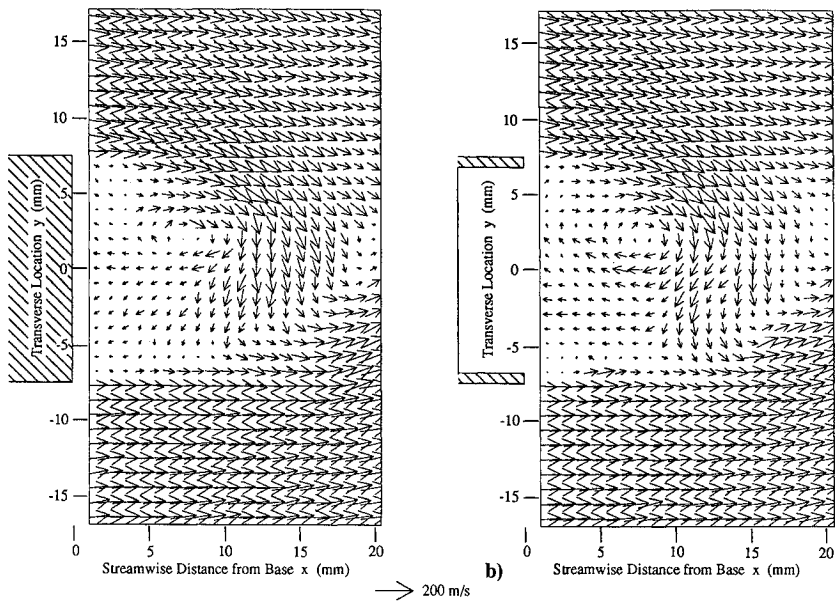

Fig. 7 Instantaneous flow structure comparison—M_∞ = 0.4 velocity vectors: a) M4b and b) M4c.

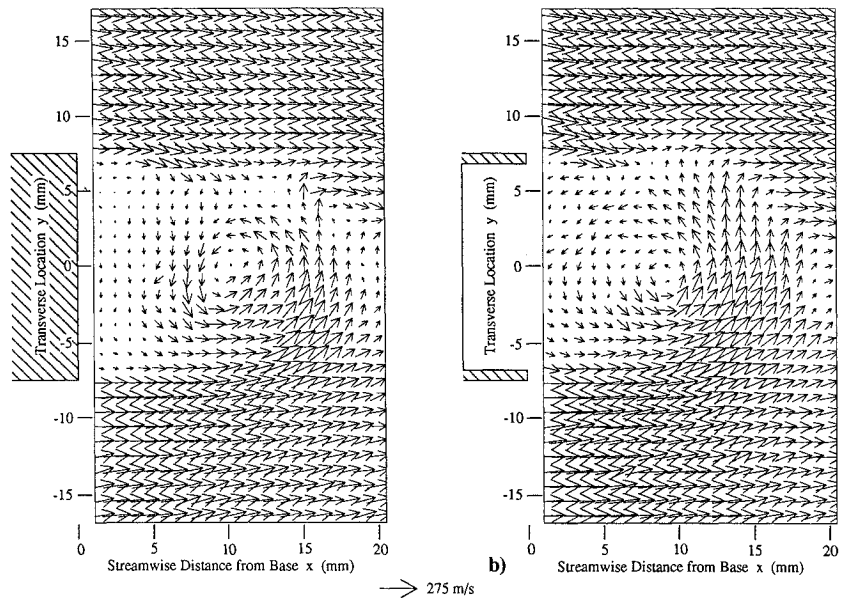

Fig. 8 Instantaneous flow structure comparison—M_∞ = 0.6 velocity vectors: a) M6b and b) M6c.

each freestream velocity condition, realizations were selected from the two base configurations with closely matching vortex locations in the near wake. Velocity vector plots for the best match from the M4b and M4c cases are shown in Fig. 7, with plots from the M6b and M6c cases shown in Fig. 8. As in Figs. 4 and 5, these velocity vector plots show only every other vector in each direction for the sake of clarity. It is evident from Figs. 7 and 8 that for each pair of realizations the center stagnation point of the first vortex downstream of the base matches to within 1 mm in each direction.

Each of these realizations, along with others not shown here, indicates that the circulating region around a fully formed vortex entering the wake covers most of the base height, which is confirmed by the results of Kruiswyk and Dutton.[4] However, in both Figs. 7 and 8, a significant difference in vortex structure due to the cavity is evident. In the presence of the base cavity, the circulating region around the fully formed vortex is extended further in all directions, diffusing the vortex motion over a larger region. Although velocity data are available only to within 1 mm of the base boundary, the vortex seems to extend partially into the cavity boundary (see first column of vectors at $x = 1$ mm and $y = -7.5$ to 7.5 mm in Figs. 7b and 8b), but the relatively small magnitude of this motion and the distance of the vortex center from the cavity preclude the vortex being significantly inhibited by the cavity walls. The extension of the vortices partially into the cavity is confirmed by tuft visualization experiments done by Kruiswyk and Dutton,[4] which showed that short strands of lightweight thread hung at the cavity boundary oscillated back and forth into the cavity in the streamwise direction, with small oscillations in the spanwise direction. However, surface flow visualization experiments performed to determine the interaction of the vortices with the inner walls of the cavity indicated very little fluid motion on the walls (i.e., very small cavity wall shear stress), even near the cavity boundary. The rms vorticity data obtained here also show no evidence of vortex formation near the cavity boundary (see Fig. 6), and so it is not likely that the vortices extend far enough into the cavity to be seriously inhibited by the cavity walls.

Another feature of the vortex expansion shown in Figs. 7 and 8 is that, with the base cavity, the vortices extend far enough across the wake to affect the opposing shear layer. For example, in Fig. 8b, the fully formed vortex shed from the lower separation point clearly interacts more strongly with the upper shear layer than is the case

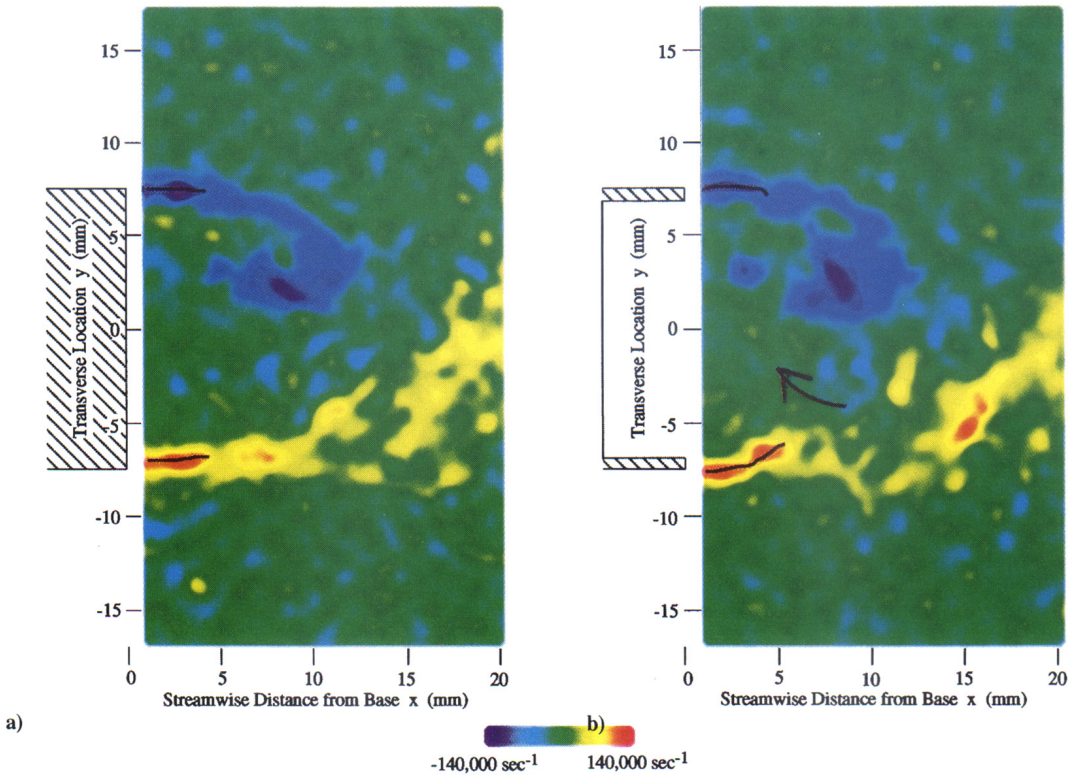

Fig. 9 Instantaneous flow structure comparison—M_∞ = 0.4 color vorticity plots: a) M4b and b) M6c.

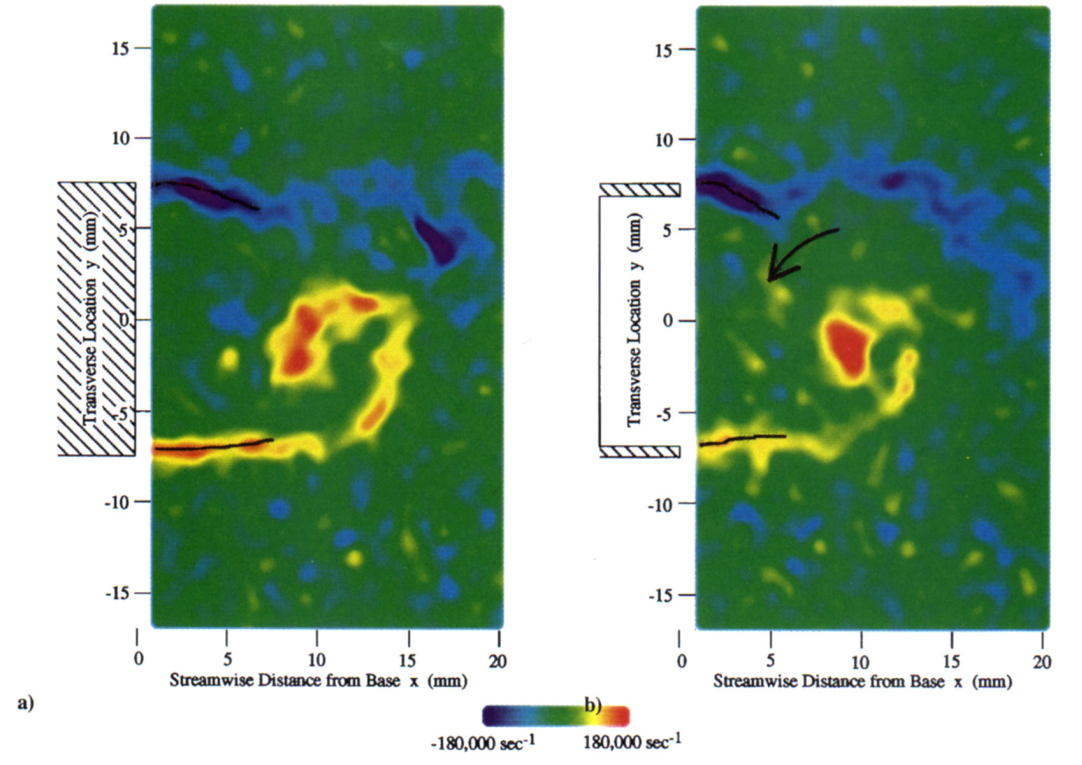

Fig. 10 Instantaneous flow structure comparison—M_∞ = 0.6 color vorticity plots: a) M6b and b) M6c.

for the blunt base in Fig. 8a. To examine this interaction, the instantaneous vorticity is plotted in Figs. 9 and 10 for each of the four realizations shown in Figs. 7 and 8. From these plots, the shear layer position can be determined and is indicated by a line in the same manner as in Fig. 6. The fluid motion near the shear layers due to vortex expansion across the wake is also shown with curved arrows. One effect from interaction of the expanded vortices with the opposing shear layers is a folding of the shear layer region toward the transverse centerline. For example, in Fig. 10b, the upper shear layer gains transverse momentum toward the centerline at locations upstream of the vortex center. The subsequent increase in shear layer curvature and convergence angle in the area upstream of the vortex center is clearly evident from both base cavity plots (lower shear layer in Fig. 9b and upper shear layer in Fig. 10b). Evidence of the vortex interaction with remnants of the shear layer downstream of the vortex center is also apparent with the corresponding motion away from the transverse centerline.

Another effect of diffused vortex motion is that increased vorticity in the area just inside of the shear layers and downstream of the separation point can reduce the local pressure, thereby increasing the

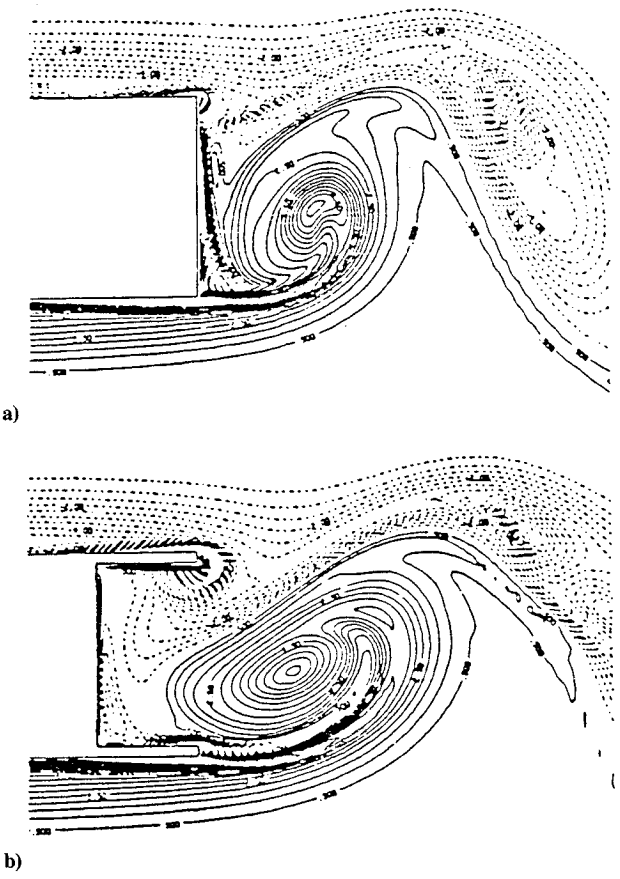

Fig. 11 Navier-Stokes numerical solution vorticity contours, taken from Rudy[10]: a) M6b and b) M6c.

curvature of the shear layer, an effect that was discussed previously. However, increases in vorticity magnitude near the shear layers that would be associated with reduced pressure are not readily apparent in Figs. 9b and 10b.

The instantaneous flow structure data can also be used for comparison to the numerical simulation of this flowfield done by Rudy.[10] This study used a time-accurate simulation of the Navier-Stokes equations to compute the laminar flow past base models similar to those used in the present experiments, with the only difference being in the transverse cavity height, which is equal to 90% of the total base height in the simulations and 80% of the base height in the present experiments. As previously mentioned, the simulations were done for freestream Mach numbers of 0.4 and 0.6 and at relatively low freestream Reynolds numbers (based on freestream velocity and base height) of 700 and 962 for Mach 0.4 and 0.6, respectively.

Instantaneous vorticity plots have been selected from the Mach 0.6 simulations (Fig. 11) that most closely match the stage of vortex development indicated by the experimental results shown in Fig. 10. In comparing the numerical and experimental results, it can be seen that there are some significant differences in the vortex structure. The lack of turbulence in the laminar flow simulations and the resultant discrepancy with the experimental flowfield (which includes small-scale turbulence and vortex fragmentation) are evident. The simulations also show that the vortices are elongated for both the blunt and cavity configurations, especially for the base cavity where the vortex stretches in the streamwise direction as it expands into the cavity, causing vortex motion far into the cavity. Additional data from Rudy[10] show distinct vortices forming near the cavity boundary at the transverse center of the wake. Although the PIV data do not extend into the cavity, the scale of the fluid motion at the boundary and the vortex formation location indicated by the experiments do not support these results. Rudy recognized the limitations of his computations and suggested future studies to include both higher Reynolds numbers and turbulence modeling to more accurately predict experimental results under typical Reynolds number conditions.

Conclusions and Summary

Analysis of the time-resolved flowfield structure in the turbulent separated wake of a base cavity has been made possible by implementation of a new particle image velocimetry (PIV) system. The data obtained have shed light on the effects of a two-dimensional base cavity and on the mechanism by which it reduces base drag.

The evidence presented indicates that the most prominent effects of a base cavity on the vortex street wake are the increased convergence of the separated shear layers from each base corner toward the transverse wake centerline, and the diffusion of vortex motion due to the expansion of individual vortices across the near wake and partially into the cavity. The diffusion of the vortices, in turn, reduces their strength by approximately 4–6%, although the vortices do not form further upstream and are not significantly inhibited by the cavity walls. This is seen at both freestream conditions examined here. It is also evident that the effects are less significant at higher freestream velocities due to the extension of the separated shear layers and the movement of the vortex formation location further downstream of the aft edge of the base, thereby reducing the effect of the cavity on the vortices. These specific effects provide the information necessary for determination of the drag reduction mechanisms of base cavities.

The apparent mechanism of the observed base cavity wake modifications depends on the replacement of the solid boundary of the blunt base with the compliant fluid boundary of the base cavity. This compliant boundary allows greater expansion of vortex motion and a resulting small increase in shear layer convergence toward the transverse centerline due to the interaction of each vortex on the upstream part of the opposite shear layer. However, vortex formation does not occur any closer to the aft edge of the base for the cavity case. These results refute the theories of Nash et al.,[2] Pollock,[3] Ringleb,[6] and Wood,[7] all of which assume that the vortices are somehow trapped or stabilized by interaction with the inner walls of the cavity. The suggestion by Compton[8] and Morel[9] that a coflowing stream sheds from the cavity wall is partially valid in that there is some momentary outflow from one edge of the cavity when vortex motion partially extends into the cavity, but the magnitude of the motion is very small and too short-lived to affect the vorticity level in the shear layer before vortex formation. This conclusion is confirmed by the surface flow experiments of Kruiswyk and Dutton[4] that indicate little or no fluid motion on the inner walls of the cavity. The proposal by Kruiswyk and Dutton[4] that periodic fluid mixing at the cavity boundary is responsible for a reduction in vortex strength is closest to being in agreement with the present results, since some mixing must occur as each vortex partly extends into the cavity, although the reduction in vortex strength is small.

Aside from the mechanisms of wake modification, one must consider the mechanism of the base pressure increase and subsequent drag reduction due to base cavities. It is true that the effects described earlier modify and slightly weaken the vortex street, which, in turn, should slightly increase the pressure in the vicinity of the vortices in the near wake. However, the wake structure changes are relatively small and the vortex formation location and path are not significantly modified. Without a significant change in the strength or location of the vortices in the near wake due to the base cavity, it seems that the most significant factor affecting the base pressure is the physical displacement of the base surface within the cavity to a position upstream of the wake, where it does not interact with the low-pressure vortices. This is the conclusion drawn by Rudy,[10] although his numerical simulations showed the vortices extending far into the cavity with corresponding effects on the wake structure.

In summary, the drag reduction mechanism of a base cavity in subsonic flow is the physical displacement of the base surface away from the vortex street wake, which is only slightly modified by the presence of the cavity.

Acknowledgments

The authors gratefully acknowledge the U.S. Army Research Office for supporting this research under Contract DAAH04-93-G-0226 with Thomas L. Doligalski as contract monitor.

References

[1]von Kármán, T., "Über den Mechanismus des Widerstandes, den ein bewegter Körper in einer Flüssigkeit erfährt," *Nachrichten von der Königlichen Gesellschaft der Wissenschaften zu Göttingen. Mathematisch-Physikalische Klasse*, 1911, pp. 509–517.

[2]Nash, J. F., Quincey, V. G., and Callinan, J., "Experiments on Two-Dimensional Base Flow at Subsonic and Transonic Speeds, British Aeronautical Research Council, ARC R&M 3427, 1963.

[3]Pollock, N., "Some Effects of Base Geometry on Two-Dimensional Base Drag at Subsonic and Transonic Speeds," Australian Aeronautical Research Lab., Aerodynamics Note 316, 1969.

[4]Kruiswyk, R. W., and Dutton, J. C., "Effects of a Base Cavity on Subsonic Near-Wake Flow," *AIAA Journal*, Vol. 28, No. 11, 1990, pp. 1885–1893.

[5]Clements, R. R., and Maull, D. J., "The Representation of Sheets of Vorticity by Discrete Vortices," *Progress in Aerospace Sciences*, Vol. 16, No. 2, 1975, pp. 129–146.

[6]Ringleb, F. O., "Separation Control by Trapped Vortices," *Boundary Layer and Flow Control*, edited by G. V. Lachmann, Pergamon Press, Oxford, England, UK, 1961, pp. 265–294.

[7]Wood, C. J., "The Effect of Lateral Vibrations on Vortex Shedding from Blunt-Based Aerofoils," *Journal of Sound and Vibration*, Vol. 14, No. 1, 1971, pp. 91–102.

[8]Compton, W. B., "Effect on Base Drag of Recessing the Bases of Conical Afterbodies at Subsonic and Transonic Speeds," NASA TN D-4821, 1968.

[9]Morel, T., "Effect of Base Cavities on the Aerodynamic Drag of an Axisymmetric Cylinder," *Aeronautical Quarterly*, Vol. 30, Pt. 2, 1979, pp. 400–412.

[10]Rudy, D. H., "A Numerical Study of Unsteady Two-Dimensional Subsonic Compressible Base Flow," Ph.D. Thesis, Dept. of Mechanical and Industrial Engineering, Univ. of Illinois at Urbana–Champaign, Urbana, IL, 1987.

[11]Little, B. H., Jr., and Cubbage, J. M., Jr., "The Development of an 8-inch by 8-inch Slotted Tunnel for Mach Numbers up to 1.28," NASA TN D-908, 1961.

[12]Molezzi, M. J., "Development and Application of Particle Image Velocimetry in High-Speed Separated Flow: Two-Dimensional Base Cavities," Ph.D. Thesis, Dept. of Mechanical and Industrial Engineering, Univ. of Illinois at Urbana–Champaign, Urbana, IL, 1993.

[13]Molezzi, M. J., and Dutton, J. C., "Application of Particle Image Velocimetry in High-Speed Separated Flows," *AIAA Journal*, Vol. 31, No. 3, 1993, pp. 438–446.

[14]Landreth, C. C., and Adrian, R. J., "Measurement and Refinement of Velocity Data Using High Image Density Analysis in Particle Image Velocimetry," *Proceedings of the Fourth International Symposium on Applications of Laser Anemometry to Fluid Mechanics* (Lisbon, Portugal), July 1988, pp. 485–497.

[15]Fage, A., and Johansen, F. C., "The Structure of Vortex Sheets," British Aeronautical Research Council, ARC R&M 1143, 1927.